Available online at www.sciencedirect.com
SCIENCE DIRECT®
Pergamon
Acta Materialia 51 (2003) 4497–4504
Acta MATERIALIA
www.actamat-journals.com

Experimental study of ordering kinetics in aluminum alloys during solidification

N. Iqbal [a,*], N.H. van Dijk [a], V.W.J. Verhoeven [a], W. Montfrooij [a], T. Hansen [b], L. Katgerman [c], G.J. Kearley [a]

[a] *Neutron Scattering and Mössbauer Spectroscopy Department, Interfaculty Reactor Institute, Delft University of Technology, Mekelweg 15, 2629 JB Delft, The Netherlands*
[b] *ILL, 6 Rue Jules Horowitz, BP 156, 38042 Grenoble cedex 9, France*
[c] *Laboratory for Materials Science, Delft University of Technology, Rotterdamseweg 137, 2628 AL Delft, The Netherlands*

Received 27 September 2002; received in revised form 11 March 2003; accepted 19 May 2003

Abstract

The microscopic structure and crystallization behavior of liquid Al and Al–0.3Ti–0.02B (wt.%) are studied by time-resolved neutron diffraction measurements during the liquid–solid phase transformation for continuous cooling. A specially developed furnace insert was used to obtain a temperature stability of 40 mK in the vicinity of the solidification temperature of T_o = 933 K. The evolution of the static structure factor $S(Q)$ has been monitored during the liquid to solid phase transformation as a function of the cooling rate. The evolution of the liquid fraction f_L during the transformation is determined from the value of the first peak in the liquid structure factor. The evolution of the solid volume fraction $f_S = 1-f_L$ is analyzed in terms of the Johnson–Mehl–Avrami model. The Avrami exponent n is found to change for pure Al as well as for Al–0.3Ti–0.02B alloy with cooling rate and the rate constant k decreases by an order of magnitude for Al–0.3Ti–0.02B alloy compared to pure Al. Anomalous temporal oscillations were observed in the Bragg peak intensity of the solid grains during the solidification of the Al–0.3Ti–0.02B alloy.

Keywords: Solidification; Aluminum alloys; Neutron diffraction; TiB_2; Structure factor

1. Introduction

The understanding and control of the microstructure evolution during the liquid to solid phase transformation in aluminum alloys is of major importance in the modern production process of tailor-made aluminum for specific applications. Accurate investigations of the liquid structure near the liquid–solid phase transformation can therefore provide useful information for the influence of the process parameters during the production process, such as cooling rate and the effect of impurities or added particles on the solidification behavior [1–3]. A significant improvement of the mechanical properties of aluminum can be obtained by the addition of small amounts of TiB_2 particles and excess titanium due to a drastic refinement of the

* Corresponding author. Tel.: +31-15-278-4533; fax: +31-15-278-8303.
E-mail address: iqbal@iri.tudelft.nl (N. Iqbal).

1359-6454/03/$30.00
doi:10.1016/S1359-6454(03)00285-4

average grain size [4,5]. Although the effect of these added grain refiners is extensively studied, the physical mechanism responsible for this grain refinement process is still not well established. It is clear from both experimental and theoretical studies [5] that micron-size TiB_2 particles strongly enhance the nucleation process of solid grains in undercooled melts. The subsequent growth of nuclei is controlled by diffusion of solute titanium and latent heat. A better understanding of the effects of solute titanium and added TiB_2 particles in the liquid–solid phase transformation of aluminum alloys is therefore highly desirable.

In the present paper, we report on time-dependent neutron diffraction measurements on the microstructure evolution of pure aluminum and Al–0.3Ti–0.02B (wt.%) alloy during the crystallization process for different continuous cooling rates.

2. Experimental

The samples used in this study were 99.999% pure aluminum (Goodfellows) and an Al–0.3Ti–0.02B (wt.%) alloy prepared from an Al–5Ti–0.2B (wt.%) commercial master alloy (KBM AFFILIPS). The particle size distribution of TiB_2 precipitates in the Al–0.3Ti–0.02B alloy was determined by optical microscopy and showed a particle size distribution in the range from 0.6 to 2.2 μm with a maximum around 1.2 μm. The pure aluminum and Al–0.3Ti–0.02B alloy samples with a mass of 10.6 g were placed in a cylindrical single-crystalline sapphire container with a height of 60 mm, an inner diameter of 10 mm, and a wall thickness of 1 mm.

The in situ neutron diffraction measurements were performed on the high-flux powder diffractometer D20 at the Institute Laue-Langevin (ILL) following a feasibility study on the disordered materials diffractometer SLAD at the Studsvik Neutron Research Laboratory (NFL). A monochromatic neutron beam with wavelength of $\lambda = 0.82$ Å and a beam height of 41 mm was used for all neutron diffraction experiments. For the high-temperature neutron diffraction measurements a dedicated vacuum furnace (7×10^{-4} mbar) was used with a vanadium heater element and a temperature stability of about 1 K.

In order to achieve the required temperature stability ($\Delta T < 50$ mK) for our solidification experiments the specially designed furnace insert of Fig. 1 was used. The furnace insert consisted of a nickel cylinder with a mass of 884 g, a height of 144 mm, and a diameter of 37 mm. The mass of the insert effectively dampens the temperature fluctuations of the main furnace and strongly improves the temperature stability. In the central part of the furnace insert a section has been cut out in order to allow a free passage of the incoming and scattered neutrons from the sample. The walls of the nickel block around the sample were covered by gadolinium in order to prevent secondary scattering. Two cartridge heaters were placed into the top and bottom part of the nickel block in order to regulate the temperature of the insert with an additional PID controller (Lake Shore model 340). The temperature of the furnace insert was monitored by a PT100 platinum resistance thermometer. By operating the main furnace in constant power mode and regulating the temperature of the furnace insert, a temperature stability of about $\Delta T \approx 40$ mK was obtained at a temperature of $T = 933$ K. The thermal response time of the furnace insert was estimated at $\tau_{ins} \approx 2$ min. For our sample geometry the expected time constant for thermal equilibrium of the sample is estimated at $\tau_{sam} \approx 5$ min.

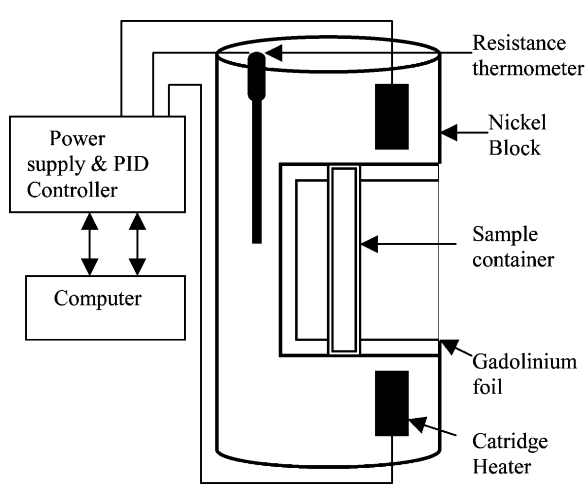

Fig. 1. Furnace insert and temperature control system for the high-stability temperature regulation close to the melting point.

3. Results and discussion

3.1. Liquid structure factor

In Fig. 2 the measured liquid structure factor $S(Q)$ as a function of the wave-vector transfer Q is shown for pure aluminum and Al–0.3Ti–0.02B alloy at a temperature of $T = 936$ K ($T > T_o$). The first peak in the liquid structure factor of pure aluminum is observed at $Q = 2.68$ Å^{-1} and has a height of $S(Q) = 2.44$. The observed structure factor is in reasonable agreement with previous neutron [6,7] and X-ray diffraction [8,9] studies of liquid aluminum in the vicinity of the solidification temperature. The measured structure factor of liquid Al–0.3Ti–0.02B alloy closely resembles the curve of pure aluminum indicating a weak influence of the alloying elements on the short-range order in the liquid. The main difference is observed in the vicinity of the first peak in the liquid structure factor. Although no significant shift in the position is observed, the height is somewhat reduced to a value of $S(Q) = 2.39$. In addition, a small peak in the structure factor of Al–0.3Ti–0.02B alloy is observed below the first liquid peak. This additional peak at $Q = 1.95$ Å^{-1} corresponds to a (0 0 1) Bragg reflection of the solid TiB_2 particles with a hexagonal crystal lattice structure in the liquid alloy.

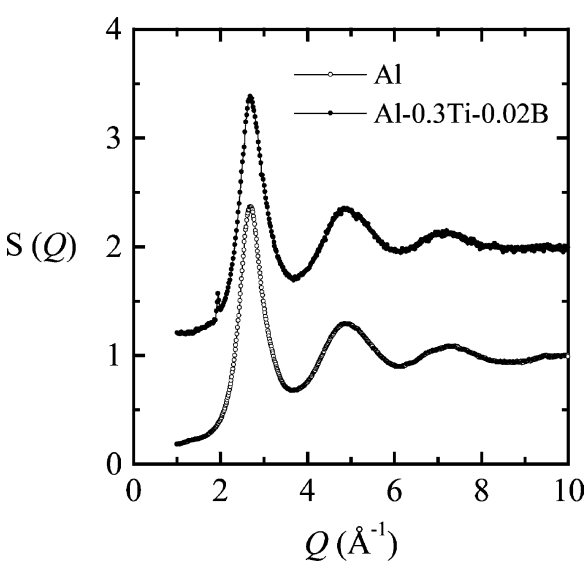

Fig. 2. Liquid structure factor $S(Q)$ as a function of the wave-vector transfer Q for pure aluminum (open circles) and Al–0.3Ti–0.02B alloy (solid circles) at a temperature of $T = 936$ K. For clarity $S(Q)$ of the Al–0.3Ti–0.02B alloy is vertically displaced by 1.

3.2. Liquid volume fraction

In order to study the influence of grain refiners on the crystallization behavior of aluminum systematic time-dependent neutron diffraction measurements of the structure factor in pure aluminum and Al–0.3Ti–0.02B alloy were performed. For each of the measurements the sample was heated to a temperature of 943 K for 1 h to obtain a homogeneous liquid phase, followed by a continuous cooling with rates of 0.06 and 0.6 K/min. During the continuous cooling the structure factor was continuously monitored by neutron diffraction in time steps of 1 min. During the liquid to solid phase transformation the liquid peaks in the structure factor (Fig. 2) gradually decrease while Bragg peaks from the solid phase emerge and grow. As the observed Bragg peak intensity strongly depends on texture in the solid phase, we use scattering from the liquid phase to determine the liquid and solid volume fractions.

Fig. 3 shows the behavior of liquid volume fraction of pure aluminum as a function of temperature for cooling rates of 0.06 and 0.6 K/min determined from the normalized variation in the structure factor $S(Q)$ at the maximum of the first liquid peak at $Q = 2.68$ Å^{-1}. For both cooling rates the transformation starts at an undercooling of about 10 K compared to the thermodynamic solidification temperature of $T_o = 933$ K. For a higher cooling rate the transformation however, extends over a wider temperature range. As a consequence, the temperature where half of the liquid volume of pure aluminum is transformed to solid ($T_{1/2}$) decreases by 4 K for a tenfold increase in the cooling rate.

In Fig. 4 the liquid volume fraction of the Al–0.3Ti–0.02B alloy is shown as a function of temperature for cooling rates of 0.06 and 0.6 K/min. Again the transformation start temperature is relatively insensitive to the cooling rate, but the transformation extends to lower temperatures at a higher cooling rate. Compared to the pure aluminum sample the liquid/solid phase transformation

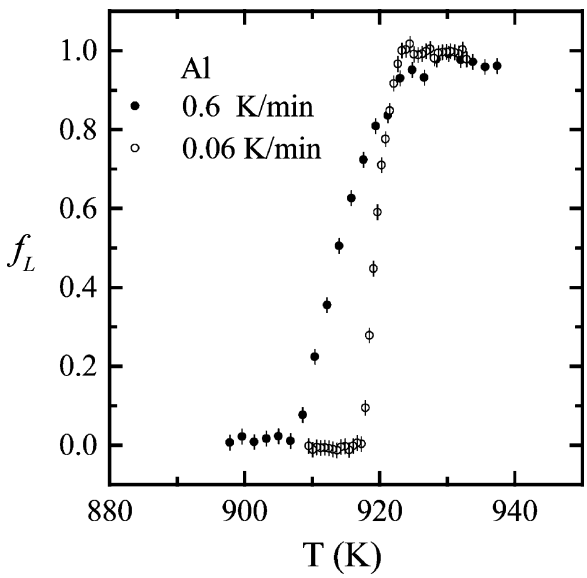

Fig. 3. Liquid volume fraction f_L of pure aluminum as a function of temperature for cooling rates of 0.06 K/min (open circles) and 0.6 K/min (solid circles). The liquid volume fraction f_L is deduced from the normalized variation in the first liquid peak in $S(Q)$ at $Q = 2.68$ Å^{-1}.

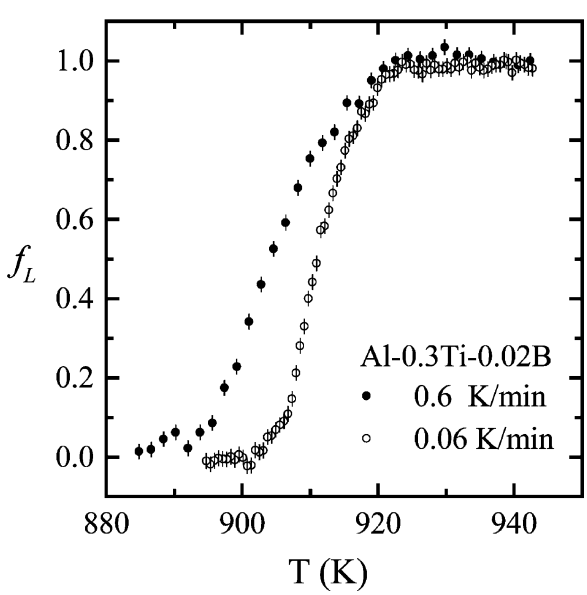

Fig. 4. Liquid volume fraction f_L of Al–0.3Ti–0.02B alloy as a function of temperature for cooling rates of 0.06 K/min (open circles) and 0.6 K/min (solid circles). The liquid volume fraction f_L is deduced from the normalized variation in the first liquid peak in $S(Q)$ at $Q = 2.68$ Å^{-1}.

of the Al–0.3Ti–0.02B alloy occurs over a wider temperature range regardless of the cooling rate. In Table 1 a summary of the experimental transformation temperatures as a function of cooling rate is given for both samples.

As expected for a phase transformation that involves latent heat, the melting/freezing transition exhibits thermal hysteresis [10]. In Fig. 5 this thermal hysteresis is clearly demonstrated in the combined heating and cooling experiments on the liquid volume fraction of the Al–0.3Ti–0.02B alloy for a heating/cooling rate of 0.6 K/min. The thermal hysteresis of the temperatures halfway the transformation is $\Delta T_{1/2} = 27$ K. The corresponding hysteresis in time amounts to $\Delta t_{1/2} = 45$ min, which is far too large to be caused by a weak thermal link between furnace insert and the sample for these low cooling rates as estimated response time of the sample amounts to $\tau_{sam} \approx 5$ min.

3.3. Transformation kinetics

The Johnson–Mehl–Avrami (JMA) model [11–14] has been widely used to describe the kinetics of isothermal phase transformations with examples in glasses [15,16], gels [17,18], polymers [19], steels [20], and metal alloys [21,22]. According to this model the fraction transformed f as a function of time t is described by the JMA equation:

$$f(t) = 1 - \exp\{-k(t - t_o)^n\}, \quad (1)$$

where k is the rate constant, t_o is the incubation time, and n the Avrami exponent. The value of the exponent n is expected to vary between 1 and 4 depending on the nucleation mechanism and the growth dimensionality [23]. For continuous cooling the transformation time t in the JMA equation can be set to zero at the time the temperature falls below the crystallization temperature $T_o = 933$ K [19]. Under the assumption that the transformation kinetics depend purely on the transformation time and independent of temperature, we can now fit the experimental data to the JMA model of Eq. (1). Provided that there is no change in the nucleation and growth mechanism during the phase transformation, the Avrami exponent n is expected to be constant [24].

In Figs. 6 and 7 the solid volume fraction $f_s(t)$,

Table 1
Transformation temperatures of pure aluminum and Al–0.3Ti–0.02B alloy at two different cooling rates, where T_s is the transformation start temperature, T_f the transformation finish temperature, $T_{1/2}$ the temperature halfway the transformation. In addition, the temperature width of the transformation $\Delta T = T_s - T_f$ and the average undercooling $T_o - T_{1/2}$ with respect to the crystallization temperature of T_o = 933 K are listed

Sample	Cooling rate (K/min)	T_s (K)	T_f (K)	$T_{1/2}$ (K)	ΔT (K)	$T_o - T_{1/2}$ (K)
Al	0.06	923	918	918	5	15
	0.60	925	907	914	18	19
Al–0.3Ti–0.02B	0.06	923	904	911	19	22
	0.60	923	894	905	29	28

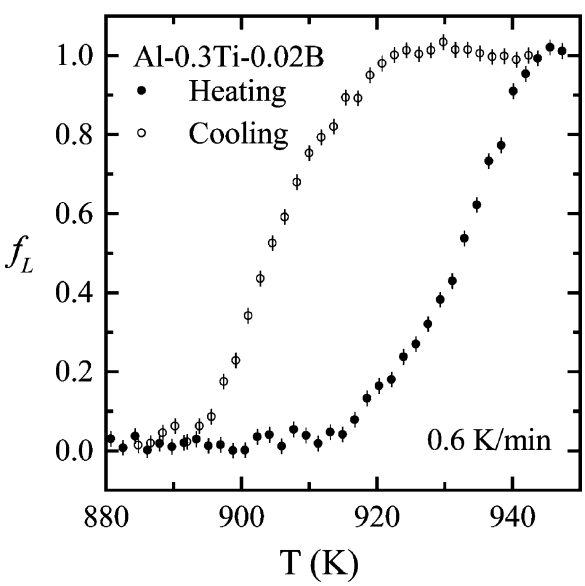

Fig. 5. Liquid volume fraction f_L of Al–0.3Ti–0.02B alloy as a function of temperature for cooling (open circles) and heating (solid circles) at a cooling rate of 0.6 K/min. The liquid volume fraction f_L is deduced from the normalized variation in the first liquid peak in $S(Q)$ at Q = 2.68 Å^{-1}.

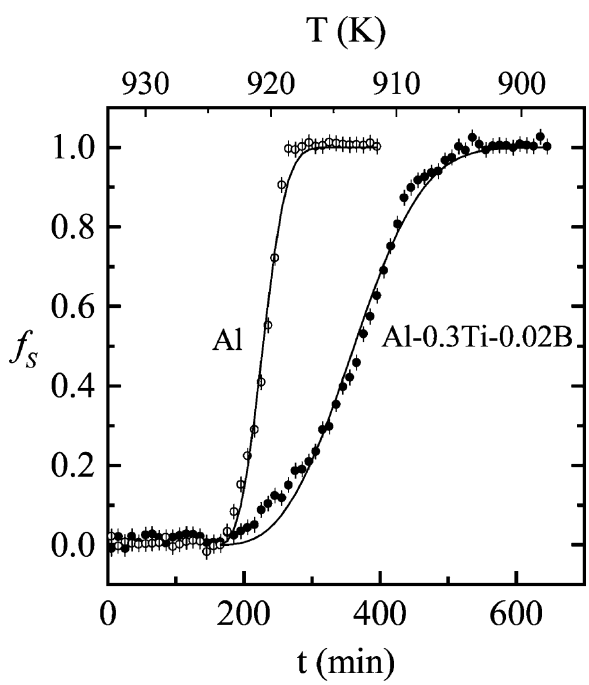

Fig. 6. Time evolution of the solid volume fraction $f_S = 1 - f_L$ for pure aluminum (open circles) and Al–0.3Ti–0.02B alloy (solid circles) at a cooling rate of 0.06 K/min. The solid line indicates a fit to the data with the Jonson–Mehl–Avrami model (see text).

deduced from the liquid fraction f_L(t), is shown as a function of time for pure aluminum and Al–0.3Ti–0.02B alloy for cooling rates of 0.06 and 0.6 K/min. The results of a fit of the JMA equation to the experimental data are listed in Table 2. The corresponding fitting curves are shown in Figs. 6 and 7. For the Al–0.3Ti–0.02B alloy fitting resulted in values of n = 2.7 and 3.1 for cooling rates of 0.06 and 0.6 K/min, respectively. For pure aluminum values n = 2.9 and 3.1 were obtained for cooling rates of 0.06 and 0.6 K/min, respectively. The rate constant, k, of the Al–0.3Ti–0.02B alloy is decreased by an order of magnitude compared to that of pure aluminum. The presence of grain refiners in the Al–0.3Ti–0.02B alloy promotes nucleation on the micron-sized substrate particles and the presence of excess titanium in the aluminum melt of the Al–0.3Ti–0.02B alloy is expected to reduce the growth rate of the crystal-

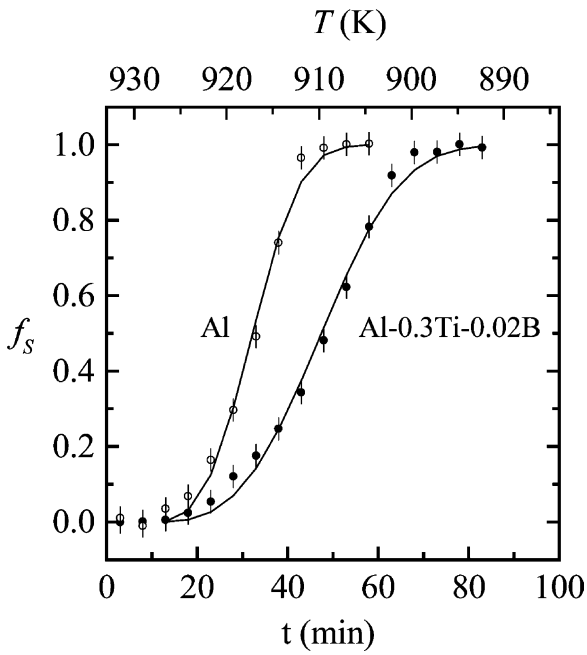

Fig. 7. Time evolution of the solid volume fraction $f_S = 1-f_L$ for pure aluminum (open circles) and Al–0.3Ti–0.02B alloy (solid circles) at a cooling rate of 0.6 K/min. The solid line indicates a fit to the data with the Jonson–Mehl–Avrami model (see text).

lites with respect to pure aluminum. Our observations are in qualitative agreement with the expected behavior of the rate constant k. The observed value of $t_{1/2}$ for pure aluminum is lower than that of Al–0.3Ti–0.02B alloy for both cooling rates confirming the relatively slow growth in Al–0.3Ti–0.02B alloy.

3.4. Growth oscillations

During the measurements of the transition kinetics of the crystallization in the Al–0.3Ti–0.02B alloy unexpected variations in the Bragg peak intensity from the crystallites were observed as a function of time. This behavior is demonstrated in Fig. 8 where the normalized Bragg peak intensity of the (1 1 1), (2 0 0), (2 2 0), and (3 1 1) reflections are shown for a continuous cooling at a rate of 0.06 K/min. For comparison the corresponding solid fraction $f_S = 1-f_L$ calculated from first liquid peak in $S(Q)$ is shown as a function of time. The observed variations in the Bragg peak intensity are found to be less pronounced for the higher cooling rate of 0.6 K/min. From Fig. 8, it is clear that no correlation in the Bragg peak intensity of the different reflections is observed. In fact, the oscillations are observed only in the Bragg peak intensity of the crystal reflections and not in the solid volume fraction, which shows a continuous increase. This behavior has not been seen in successive measurements on pure aluminum.

The observed oscillatory behavior cannot be due to mechanical vibrations of the sample cell or to fluctuations in the sample temperature, which is controlled to within 40 mK. It is probable, that the fluctuations observed in the Bragg peak intensity are intrinsic to the growth kinetics of the crystallites in the Al–0.3Ti–0.02B alloy itself. One interpretation of these observations is that the crystal growth in the Al–0.3Ti–0.02B alloy is diffusion limited due to the latent heat released by the crystallization. The subsequent increase in the local

Table 2
Transformation parameters of pure aluminum and Al–0.3Ti–0.02B alloy at two different cooling rates obtained from a fit of the experimental liquid volume fraction to the JMA model, where n is the Avrami exponent, k is the rate constant, t_o is the transformation start time, and $t_{1/2}-t_o = [\ln(2)/k]^{1/n}$ is the time halfway the transformation after the start of the transformation. The time when the temperature falls below the crystallization temperature $T_o = 933$ K is chosen as $t = 0$

Sample	Cooling rate (K/min)	n	k (min^{-n})	t_o (min)	$t_{1/2}-t_o$ (min)
Al	0.06	2.9(3)	$3.3(4) \times 10^{-6}$	160	67.6
	0.60	3.1(1)	$5.0(5) \times 10^{-5}$	10	21.9
Al–0.3Ti–0.02B	0.06	2.7(1)	$5.0(4) \times 10^{-7}$	160	197.4
	0.60	3.1(1)	$9.1(2) \times 10^{-6}$	10	37.4

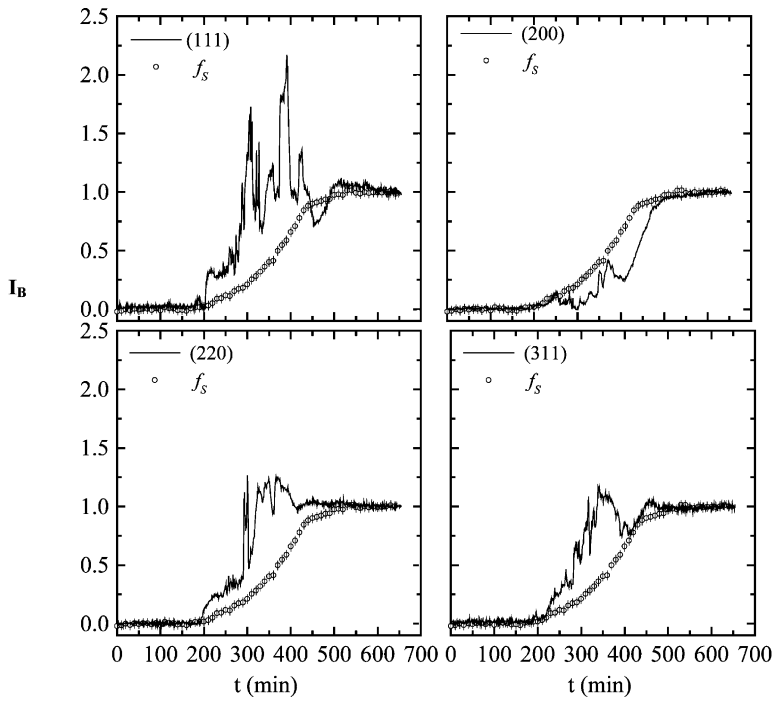

Fig. 8. Normalized integrated Bragg peak intensity I_B for the (1 1 1), (2 0 0), (2 2 0), and (3 1 1) reflections of fcc aluminum of Al–0.3Ti–0.02B alloy as a function of the time t for a cooling rate of 0.06 K/min. For comparison the time evolution of the solid volume fraction $f_S = 1-f_L$ deduced from the variation in the first liquid peak in $S(Q)$ is shown. The temporal fluctuations observed in the Bragg peak intensities of the grains are not reflected in the volume fraction of the solid phase.

sample temperature is expected to have a strong effect on the growth rate (recalescence).

In the absence of a true powder average, the fluctuations in Bragg peak intensity may however, also be due to a random motion of individual crystallites. For rotating crystallites the reflection condition in the scattering plane of the detector is only fulfilled for short periods of time. This interpretation seems unlikely given the quasi-periodic nature of oscillations. Also the relative size of the oscillations seems too large for the expected number of grains in reflection. For an illuminated sample volume of about 3 cm^3 and a final grain diameter of about 500 μm the number of crystallites present during the transformation is of the order of 5×10^4. From the size of the (1 1 1) Bragg peak intensity relative to the main liquid peak an average number of $N \approx 300$ grains was estimated to be in reflection for a cooling rate of 0.06 K/min. As a result the relative fluctuations in Bragg intensity are expected to be of the order of $1/\sqrt{N} \approx 6\%$, which is much smaller than the observed oscillations.

4. Conclusions

The paper presents the structural and kinetic features of the crystallization kinetics in pure aluminum and an Al–0.3Ti–0.02B alloy with TiB_2 grain refiners. The results can be summarized as follows:

(1) The short-range order in pure aluminum and Al–0.3Ti–0.02B alloy is continuous at the freezing transition. The transformation process is spread over several degrees in temperature. The dynamic freezing range was observed to increase with the addition of nucleating agents.
(2) The kinetics of the liquid to solid phase transformation is found to be strongly dependent on the presence of TiB_2 grain refiners and the excess titanium. For Al–0.3Ti–0.02B alloy

grain growth is three-dimensional and the growth rate is observed to decrease by an order of magnitude compared to the growth rate observed for pure aluminum.

(3) Although the liquid fraction varies continuously during solidification, the Bragg peak intensity of the crystal reflections shows remarkable temporal fluctuations for the Al–0.3Ti–0.02B alloy. This phenomenon appears to be intrinsic to the material under study.

Acknowledgements

We thank R. Delaplane and R. McGreevy for their assistance during the preliminary measurements at the Studsvik Neutron Research Laboratory. The Institute Laue-Langevin is gratefully acknowledged for the beam time to perform these neutron diffraction experiments. We thank P. van der Ende for the design of the furnace insert. This work was financed in part by the Netherlands Foundation for Fundamental Research of Matter (FOM) and the Netherlands Institute for Metals Research (NIMR).

References

[1] Shannon RF, Glavicic MG, Singh MA. J Macromol Sci 1994;B33:357.
[2] Allen CM, O'Reilly KAQ, Cantor B, Evans PV. Mater Sci Eng 1997;A226-228:784.
[3] Xing LQ, Hufnagel TC, Eckert J, Loser W, Schulz L. Appl Phys Lett 2000;77:1970.
[4] Cisse J, Kerr HW, Bolling GF. Metal Trans 1974;5:633.
[5] Easton M, Stjohn D. Met MaterTrans 1999;A30:1625.
[6] Takeda S, Kawakita Y, Inu M, Maruyama K, Tamaki S, Waseda Y. J Non-Cryst Sol 1996;205-207:365.
[7] Takeda S, Harada S, Tamaki S, Waseda Y. J Phys Soc Jpn 1991;60:2241.
[8] Waseda Y. The structure of non-crystalline materials. New York: McGraw-Hill, 1980.
[9] IAMP database of SCM-LIQ, Tohoku University. Available at: http://www.iamp.tohoku.ac.jp/database/scm/LIQ/sq.html.
[10] Herhold AB, King HE, Sirota EB. J Chem Phys 2002;116:9036.
[11] Johnson J, Mehl R. Trans AIME 1939;135:416.
[12] Avrami M. J Chem Phys 1939;7:1103.
[13] Avrami M. J Chem Phys 1940;8:212.
[14] Avrami M. J Chem Phys 1941;9:177.
[15] Sung YM, Kim S. J Mater Sci 2000;35:4293.
[16] Gualtieri AF, Mazzucato E, Tang CC, Cernik R. J Mater Sci Forum 2000;312:224.
[17] Fogg AM, Price SJ, Francis JJ, O' Brien S, O'Hare D. J Mater Chem 2000;10:2355.
[18] Malek J. Thermochem Acta 2000;355:239.
[19] Supaphol P. J Appl Polym Sci 2000;78:338.
[20] Louzguine DV, Inoue A. J Mater Sci 2000;35:4159.
[21] Lee JK, Choi G, Kim DH, Kim WT. Appl Phys Lett 2000;77:978.
[22] Imbert CAC, MacQueen H. J Mater Sci Technol 2000;16:532.
[23] Henderson DW. J Thermal Anal 1979;15:325.
[24] Porter DA, Easterling KE. Phase transformation in metals and alloys. London: Champan & Hall, 1993.